

School of Psychology  
University of Nottingham  
Nottingham  
United Kingdom



**Building a computational model of the visual system to investigate temporal  
harmonics in modulated visual stimuli**

**Kamyab Mirhosseini**

20303625

MSc Computational Neuroscience, Cognition and AI  
Supervisor: Dr Jonathan Patrick

September 15, 2021

## **Abstract**

Peripheral vision is an important aspect when it comes to studying vision as it makes up the majority of the visual field. Therefore when one part of the visual system such as the central vision is impaired, it is crucial to be able to use different techniques to use the remaining of the visual field for all daily tasks. Disorders such as age-related macular degeneration suffer from losing central vision, hence, these patients evolve new eye movements and strategies to use the remaining of the visual field for different tasks. Meanwhile, visual scientists attempt to develop new methods to further improve the use of the remaining vision in visual disorders. Some of these approaches include manipulating visual targets' dynamics by introducing temporal modulations that can create temporal harmonics to widen the spatio-temporal range of the stimuli and improve peripheral acuity. In this study we attempt to build a model of the visual system in order to investigate whether temporal harmonics are indeed involved in improving peripheral acuity in two specific approaches; subsampling the stimuli and contrast polarity reversal of the stimuli. We also made comparisons between the model estimations and human data to draw further interpretations about temporal harmonics' effects on vision. We found that the model replicates certain aspects of the visual system such as the threshold of spatial and temporal frequencies and visibility is better in unmodulated stimuli. The model is a suitable foundation that can be expanded on by future experimentation and to reach a more complete representation of the visual system.

# Contents

<b>1</b>	<b>Introduction</b>	<b>3</b>
<b>2</b>	<b>Methods and Materials</b>	<b>5</b>
2.1	Recreating the Stimuli . . . . .	5
2.2	Plotting the Window of Visibility (WoV)(Kelly, 1979) . . . . .	6
2.3	Improving the WoV . . . . .	6
2.4	Fourier Transform of the Stimuli . . . . .	6
2.5	Combining the FT and WoV . . . . .	7
<b>3</b>	<b>Results</b>	<b>7</b>
3.1	Plotting and Improving the Window of Visibility (WoV)(Kelly, 1979) . . . . .	7
3.2	Fourier Transform of the Stimuli . . . . .	9
3.3	Combining the FT and WoV . . . . .	11
<b>4</b>	<b>Discussion</b>	<b>14</b>
4.1	Summary . . . . .	14
4.2	Interpretations, Limitations and Future Directions . . . . .	15
<b>5</b>	<b>Appendix</b>	<b>18</b>
5.1	MATLAB code . . . . .	18
5.1.1	WoV . . . . .	18
5.1.2	Fourier Transform of one unmodulated stimulus . . . . .	18
5.2	Tables of all the original results . . . . .	19
5.2.1	Unmodulated Results . . . . .	19
5.2.2	Subsampled Results . . . . .	19
5.2.3	CPR Results . . . . .	20

# 1 Introduction

Peripheral vision or indirect vision refers to visuals that are perceived outside of the point of fixation. Peripheral vision which is what makes up the majority of the visual field is itself made up of 3 different sections. The far-peripheral, mid-peripheral and near-peripheral are distanced from the centre of gaze accordingly (Strasburger et al., 2011). It has been found that with the increase of the retinal eccentricity of a visual stimulus, the spatial details of the stimulus are perceived less (Demirel et al., 2012).

According to Owen et al. (2012) an estimate of 5% of all visual disabilities and blindness over the age of 65, in the UK is caused by Age-related macular degeneration disorder (AMD). AMD which comes with loss of central vision would lead the patient to rely on peripheral vision, therefore impairment on vision is observed when completing high spatial detail tasks.

Visual tasks that involve solving tasks with high spatial details are tasks such as recognition of faces and reading which are reliant on central vision. Therefore the loss of the central vision can be consequential to the functionality of these tasks resulting in an involuntary use of the peripheral vision for these tasks, even though spatial details are poor with higher retinal eccentricity. Therefore, the eyes will have to contrive new strategies and movements to use peripheral vision for high spatial tasks. Peripheral vision is known to be weak in humans because of the lower density of the ganglion cells on the outer areas of the retina, (Strasburger et al., 2011), however, with developing new approaches, peripheral vision can be involved in improving vision in populations that are diagnosed with visual disorders such as age-related macular degeneration or other diseases that limit foveal function such as central scotoma. These improvements can be the result of heavily relying on peripheral vision with the use of eye movements in order to perform tasks that involve focus and high spatial tasks. This is due to the fact that central vision loss diseases are majorly permanent and vision will automatically evolve other appropriate approaches. Preferred Retinal Locus (PRL) refers to an area of the retina which is used as a pseudofovea instead when central vision is impaired, and it is used regularly in designing rehabilitation exercises for MD and central scotoma patients (Crossland et al., 2005), even though it does not restore vision completely and some visual tasks still remain poor.

Because of these newly formed eye movements that cope with high spatial tasks, macular disease patients also develop involuntary eye movements, also known as fixational eye movements (FEMs), when trying to fixate on visual stimuli (Kumar and Chung, 2014) and produce a stochastic range of motions of the visuals on the retina that can have a range of different speeds and movements. Falkenberg et al. (2007) had found that these involuntary movements and difficulties with fixation also contribute to a variety of visual losses AMD patients experience.

These fixational eye movements, however, in normal vision scenarios have been shown to be beneficial to visual acuity. For example, when the eyes fixate on a point of fixation and a visual target is presented in the peripheral field, using slow drifts to move the target around in the peripheral field in order to reach the most sensitive area of the retina (Nachmias, 1961) would result in improving acuity. Additionally, according to a study by Martinez-Conde et al. (2006), one of the ways to prevent fading during fixation due to neural adaptation, is to jitter the stimulus in order to stimulate the retina further, which would introduce additional information to the retina and help improve acuity of the visual target. Fixational drifts have also been found to transfer spatial detail into the temporal domain (Boi et al., 2017). This means that when the eyes are fixated on a point of

fixation and a target is in the peripheral field, by drifting the eyes and moving the target in the peripheral field, the spatial details of the stimulus are repeated in different positions and therefore temporal information is introduced across a range of time steps.

These findings, coupled with the fact that majority of research on peripheral vision had been on stationary images and not in-motion stimuli, motivated Patrick et al. (2019) to use these benefits of fixational eye movements and temporal information to produce temporal harmonics to peripheral stimuli. This means that by introducing temporal modulations to the stimuli, and controlling the temporal information that are inputted in the visual system, temporal harmonics can be generated across a range of different time steps and therefore additional information would be available to the retina that would ultimately result in improved acuity (Patrick et al., 2019). Two different methods were proposed to control the temporal information by modulating the stimuli. The first approach was to subsample the visual target, meaning that the visual target is introduced in the peripheral field in evenly spaced intervals rather than constant exposure. The second method proposed was contrast polarity reversal (CPR), which is reversing the contrast of the visual target in the peripheral field.

When introducing temporal modulations using the methods proposed, it is important to note that in order to be able to use information resulted by temporal modulations of stimuli, the information must fall within the observers spatio-temporal contrast sensitivity function (Kelly, 1979), also known as the Window of Visibility (WoV) (Watson et al., 1986; Watson, 2013), because manipulating the temporal components of the stimuli would cause a range of different contrasts. Contrast sensitivity which is defined as the sense of perceiving the difference between the luminance of an object as opposed to its environment, is important when trying to detect a visual stimulus (Chung and Legge, 2016).

The spatio-temporal threshold surface for contrast sensitivity was measured and plotted by Kelly (1979), which is today known as the spatio-temporal contrast sensitivity function (WoV), and is well-known in the movie industry. Watson (2013) conducted a detailed study on the response of the human visual system to high frame rates and the threshold at which different artifacts such as motion, blur, and most importantly for this study, the sample artifact are perceived visually. Using Fourier Transforms to look into the frequency domain of the visual targets, they were able to observe harmonics across the temporal axis of the Fourier transform when sampling artifact was applied.

Therefore Patrick et al. (2019) designed their experiment where both subsampling and CPR stimuli are compared to unmodulated stimuli. Different speeds and positions of the peripheral target at different modulation conditions were also tested in the experiment. They found that contrast polarity reversal improves peripheral acuity at all speeds whereas subsampling the stimuli improves acuity only in high speed but impairs peripheral vision at lower speeds (Patrick et al., 2019).

One of the interpretations that can explain why visual improvement occurs in these experiments is that by introducing these temporal harmonics via modulations, the spatio-temporal information that is inputted into the visual system are expanded, (Watson, 2013), hence we observe improvement in peripheral acuity. Therefore in this study, we attempt to model this explanation by building a model of the visual system and similarly to Watson (2013) we do Fourier transform of all conditions of the Patrick et al. (2019) experiment. The window of visibility function is plotted and modernised in order to make sure the information obtained from the Fourier Transform of the stimuli fall within the spatio-temporal contrast sensitivity function and that observers are

actually sensitive to high temporal frequency signals. Using the Fourier transform function, the content of each condition (including its temporal domain) is computed and plotted against the window of visibility, and collapsed into single of so called 'estimate of visibility' which determined the performance of the model but also used to compare the model with human data.

## 2 Methods and Materials

In order to build a computational model of the visual system, we started by building the window of visibility and modernising it with accurate values collected from the plot of each of its components. Then we would do a Fourier transform of the recreated stimuli for each condition and speed and fit the results to the window of visibility to find out the available information that the human eye is sensitive to, in a single value that gives an estimate of visibility of the visual target. At the end we compared these estimations of visibility values that were produced from the model with real human data.

### 2.1 Recreating the Stimuli

The stimuli were recreated according to the study by Patrick et al. (2019) with three different conditions each including 6 different speeds. The conditions of the study include unmodulated stimuli, contrast polarity reversal and subsampled stimuli. The stimuli were created with PsychoPy v2021.2.3 (Peirce, 2007). The positions of the stimuli were converted from the Patrick et al. (2019) paper in order to keep the consistency the same. For each of the three conditions, six different speeds were used and each trial consisted of 25 images. Each frame included a fixational cross for the participants to fixate their vision and a Landolt ring on the right side in the peripheral field. For the unmodulated condition, the Landolt ring appeared in every frame with a fixed contrast (Figure 1; Top line). In the subsampled condition, the stimulus was presented in evenly spaced out intervals, meaning that the stimulus was absent for every second, third, and fifth frame respectively as seen in Figure 1. For the contrast polarity reversal (CPR) condition, the contrast of the stimuli was reversed in different orders as seen in Figure 2. The different inter-stimulus intervals in the subsampled and CPR condition are referred to as 'modulation conditions'.

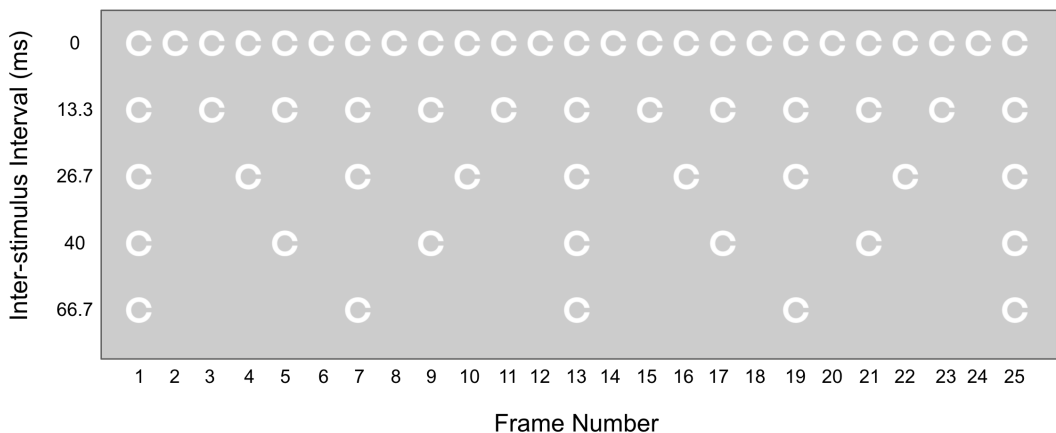


**Figure 1:** **Top line:** The Unmodulated condition **Bottom 4 lines:** The order of the subsampled condition

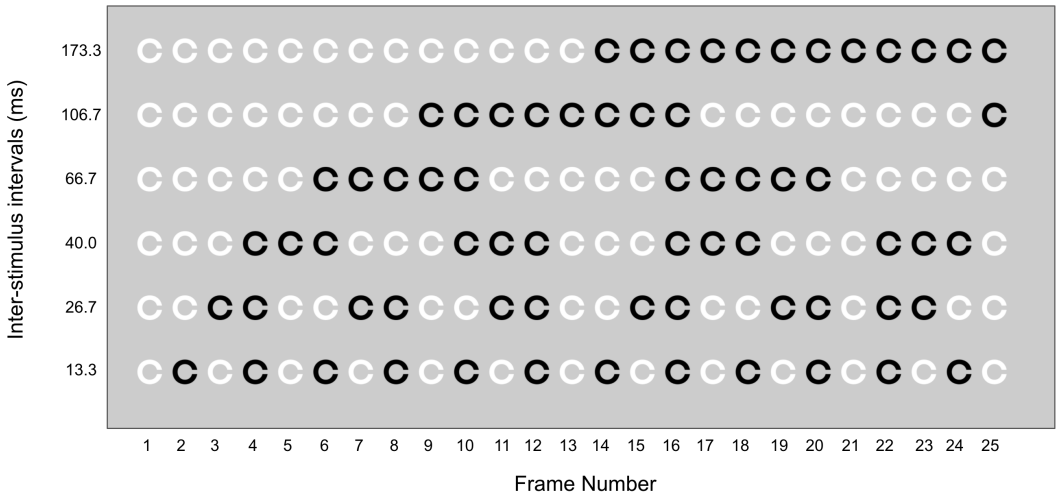


**Figure 2:** The order of the CPR condition stimuli

## 2.2 Plotting the Window of Visibility (WoV)(Kelly, 1979)

The original Window of visibility was plotted in MATLAB by using the spatio-temporal contrast sensitivity function obtained from Kelly (1979) (Equation 1), however, the constants of this function were modernised and improved at the next stage.

$$G(\alpha, \nu) = [6.1 + 7.3|\log(\nu/3)|^3] \times \nu\alpha^2 \exp[-2\alpha(\nu + 2)/45.9] \quad (1)$$

In order to plot the 3D surface, Equation 1 was rearrange by substituting the the  $\nu$  variable by  $\nu = \omega/\alpha$  where  $\omega$  represents temporal frequency and  $\alpha$  is the spatial frequency.  $G$  which is the output of the function represents the height of the surface.

## 2.3 Improving the WoV

In order to improve the WoV function, the function was broken up into its original components, such that

$$G(\alpha, \nu) = \kappa\nu\alpha^2 \exp(-2\alpha/\alpha_{max}) \quad \kappa = 6.1 + 7.3|\log(\nu/3)|^3 \quad \alpha_{max} = 45.9/(\nu + 2)$$

Using the software Data Thief v1.7, the graphs corresponding to each of the variables were used to collect data points according to the plot taken from Kelly (1979). To improve the constants of the equation for  $\kappa$ , we used Figure 8 of the Kelly (1979) paper where scale factor  $\kappa$  is plotted against log-velocity. Similarly, to improve the  $\alpha_{max}$  equation, we used Figure 6 of the Kelly (1979) paper and collected the positions of the peak points of each of the contrast sensitivity curves. The collected points were then used in GraphPad Prism v9 with a curve fitting tool that fitted a curve to the points collected and computed the best-fit values of the constant values of the equations.

## 2.4 Fourier Transform of the Stimuli

The Fourier transform of the stimuli were also computed on MATLAB. Each batch of 25 images which makes up one trial was loaded and converted into a 3D matrix of the pixel values of each image and a  $z - axis$  of size 25, where 1-25 represents each image frame. A 3D Fourier transform was implemented on the 3D matrix as a whole using the MATLAB function (fftn). The result of each Fourier transform was then converted into a

2D matrix by taking the mean of all columns of each image, producing a  $1800 \times 25$  matrix. This process was repeated for every trial in the unmodulated, subsampled and CPR conditions.

## 2.5 Combining the FT and WoV

In order to combine the Fourier transform with the window of visibility, the values that form the window of visibility were normalised by being divided by their maximum value. As the WoV goes from zero to positive on both axis, we extracted the positive quadrant of the Fourier transform matrix in order to match the positive axis of the WoV, and multiplied the positive quadrant by the normalised WoV matrix resulting in another 2D matrix. This matrix was then also converted into a single value by doing a sum of the whole matrix, which would give us an estimation of visibility. This process was repeated for all conditions and speeds and the values were normalised with respect to the unmodulated condition at speed 0. The values for the estimate of visibility shown in Table 1, are used to make comparisons with the human data. However at this stage we compare only the 66ms ISI modulation condition to compare our results with human data because this modulation condition showed the best performance in humans.

## 3 Results

The aim of this study was to investigate whether temporal harmonics increase the amount of information within the WoV and cause an improvement in peripheral acuity when performing tasks on contrast polarity reversal and subsampled stimuli. The following results are the original and the modernised spatio-temporal threshold surface, the Fourier transform of the visual stimuli, a table of all the resulted estimation of visibility for all conditions and a comparison between the model results and human data.

### 3.1 Plotting and Improving the Window of Visibility (WoV)(Kelly, 1979)

First we plotted the window of visibility according to the original function (Equation 1) which produces a 3D surface called the spatio-temporal threshold surface (Figure 3A).

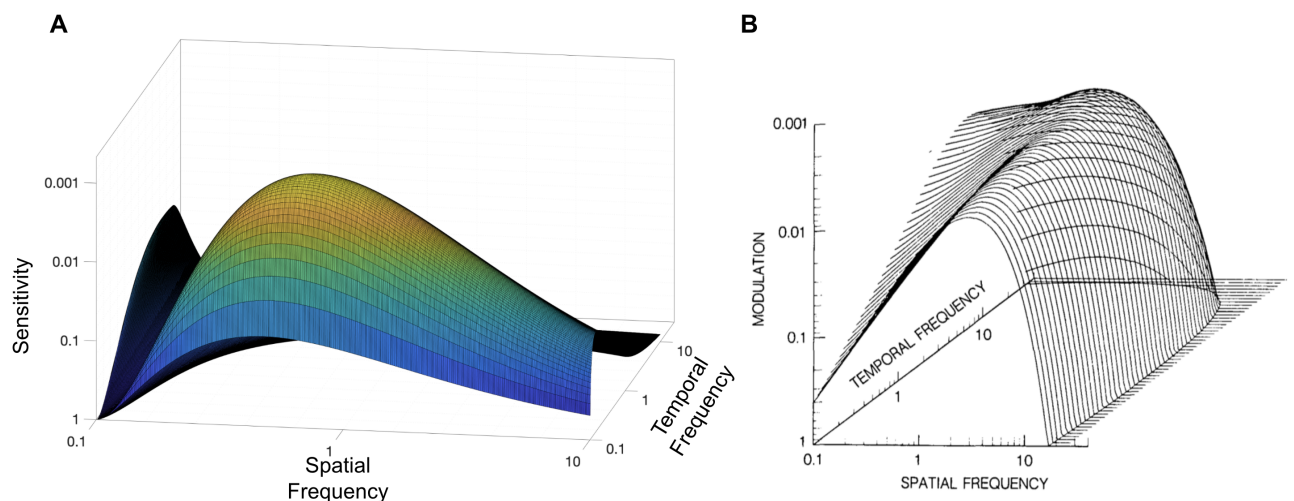


**Figure 3:** (A) The spatio-temporal threshold surface plotted from Equation 1 (B) The original spatio-temporal threshold surface (WoV) by (Kelly, 1979)

This figure has the spatial frequency on the x-axis and the temporal frequency on the y-axis. The human eye sensitivity is therefore represented on the z-axis. We can use this plot as a basic threshold for the human contrast sensitivity, however, in order to attain more accurate results and use modern ways to improve the spatio-temporal threshold surface, we collected data points from the spatial frequency curves in the Kelly (1979) paper (Figure 4B and 5B) and fit a curve through them to obtain new best-fit constant values. The curve-fit resulted in the function as a whole to change slightly with the new values as seen below:

$$\kappa = 25.89 + 28.46|\log(\nu/3)|^{3.034} \quad (2)$$

The new equation for  $\kappa$  was fitted using the figure 8 of the Kelly (1979) paper as seen here in Figure 4B. About 70 data points were collected using Datathief.jar with which the curve in Figure 4A was fitted.

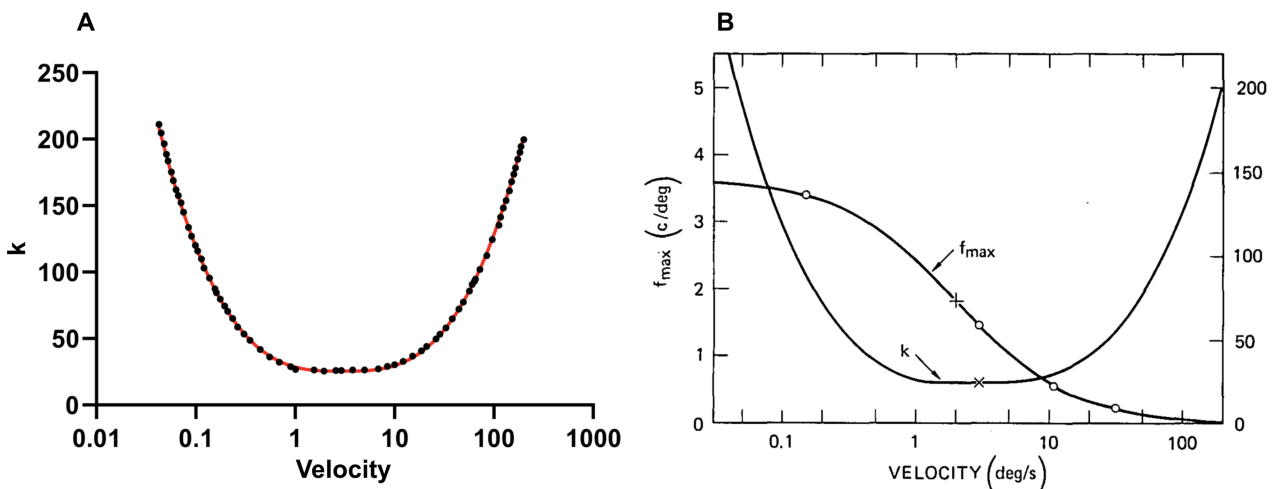


**Figure 4:** (A) The best-fit curve on the data collected for  $\kappa$  from the  $\kappa$  plot on (B)

Using the peak frequencies of the spatial frequency curves measured in figure 6 of the Kelly (1979) paper (Figure 5B) we were able to plot another best-fit curve to obtain a more accurate function for  $\alpha_{max}$  (Figure 5A).

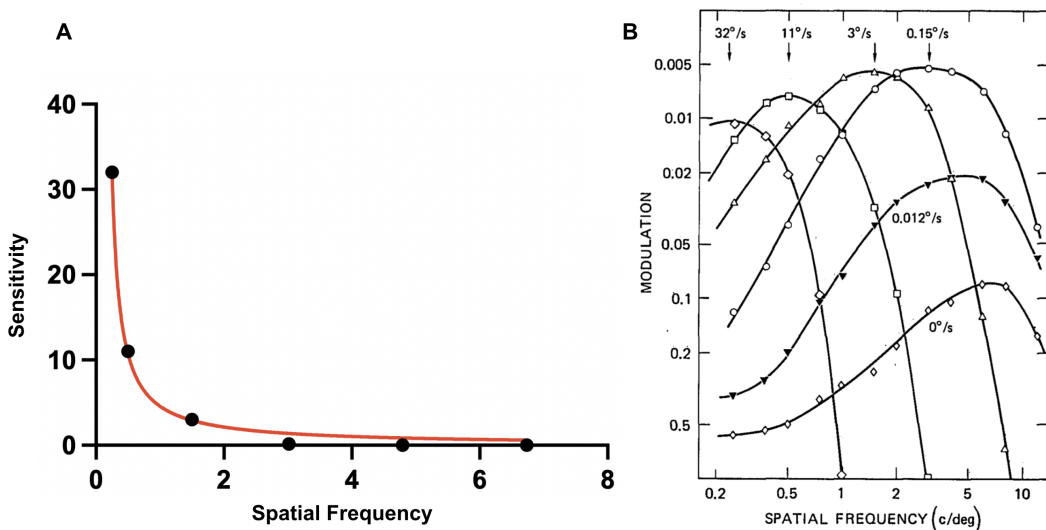


**Figure 5:** (A) The best-fit curve on the data collected from the peak points for  $\alpha_{max}$  from (B)

These best-fit values changed the  $\alpha_{max}$  equation to the equation below with new constant values of 4.004 and 0.1256.

$$\alpha_{max} = 4.004/(\nu - 0.1256) \quad (3)$$

Therefore, now by combining all the new equations, which is substituting Equation 3 & 4 into the original  $G$  function in section 2.3, the function to plot the surface as a whole changed into:

$$G(\alpha, \nu) = [25.89 + 28.46|\log(\nu/3)|^{3.034}] \times \nu\alpha^2 \exp[-2\alpha(\nu - 0.1256)/4.004] \quad (4)$$

The newly refined function was then used to plot a new spatio-temporal threshold surface that produced a slightly different WoV as seen in Figure 6.

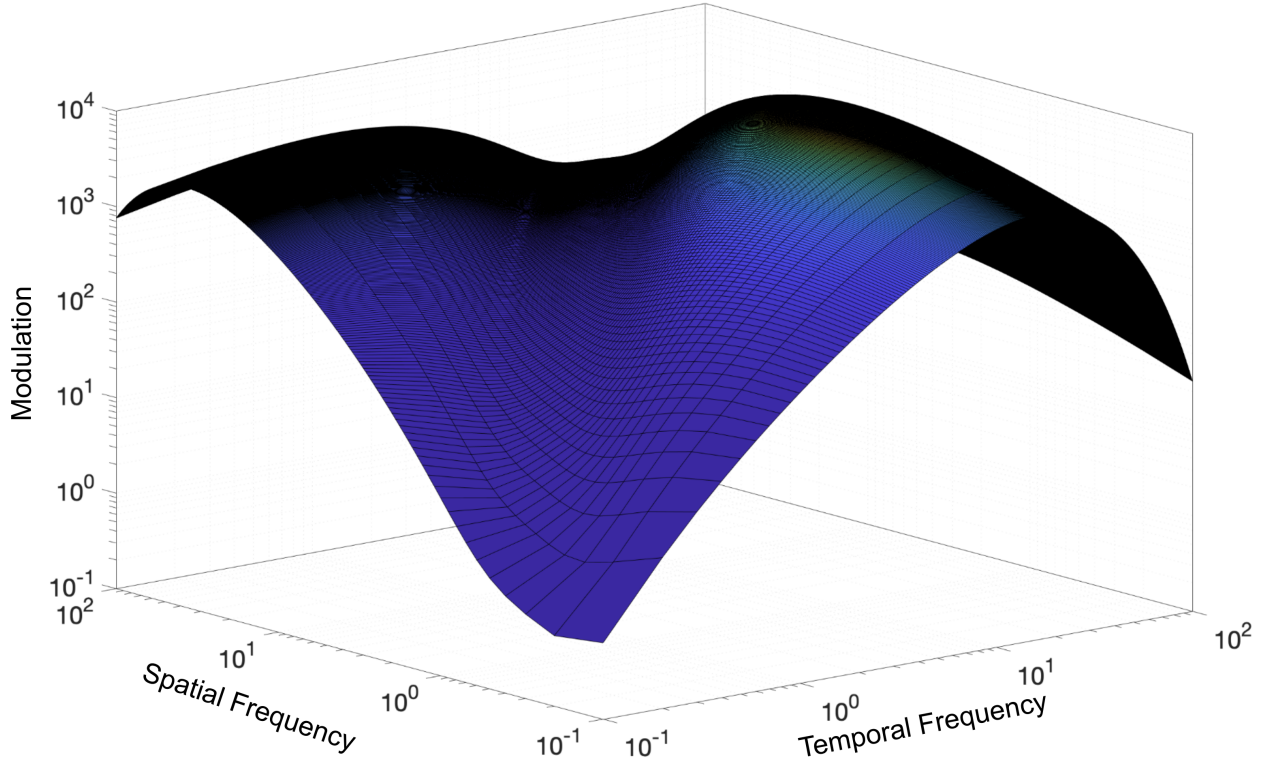


**Figure 6:** The refined spatio-temporal threshold surface

### 3.2 Fourier Transform of the Stimuli

At the next stage we computed the Fourier transform of each trial of the experiment in each condition and collapsed the resulted 3D matrix into a 2D matrix of  $1800 \times 25$ . The plots below are examples of the 2D Fourier transform of unmodulated stimuli (Figure 7), subsampled stimuli at 66ms ISI (Figure 8) and CPR condition at 66ms ISI (Figure 9). The temporal frequency is the different frames of a trial which is along the x-axis and the spatial frequency is represented along the y-axis.

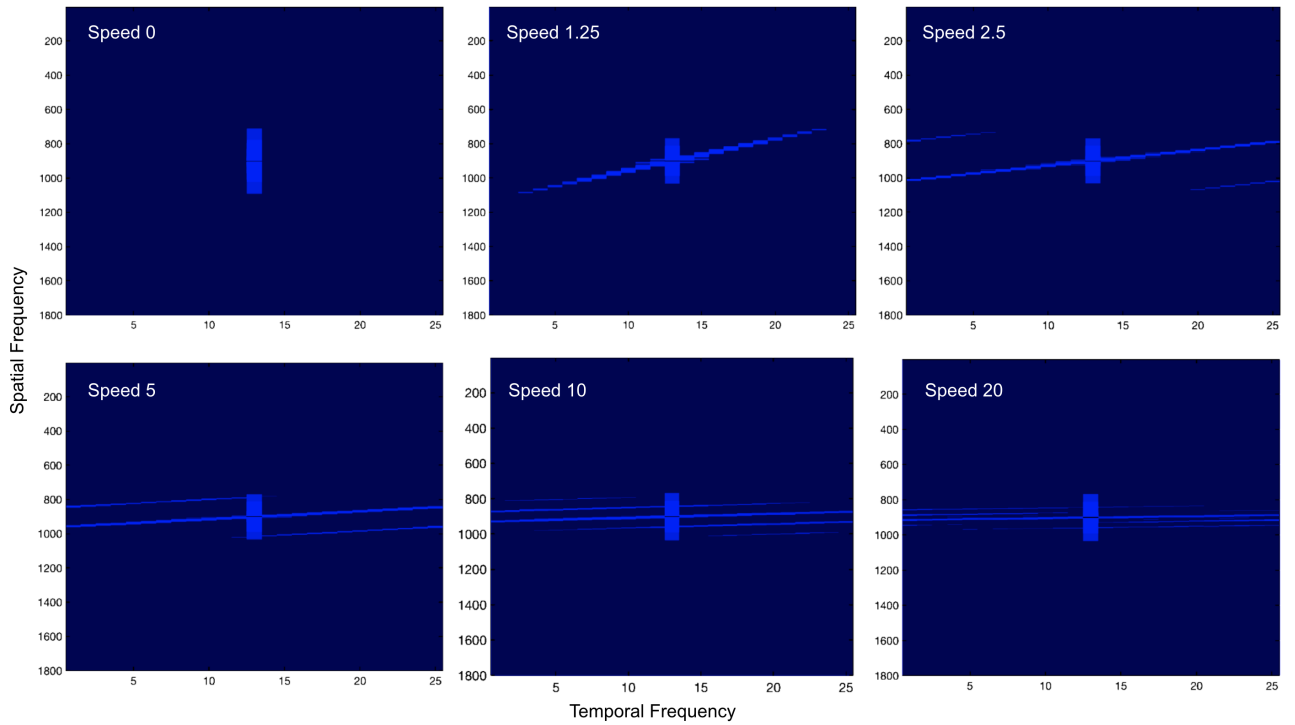


**Figure 7:** Fourier transform of the unmodulated stimuli at 6 different speeds

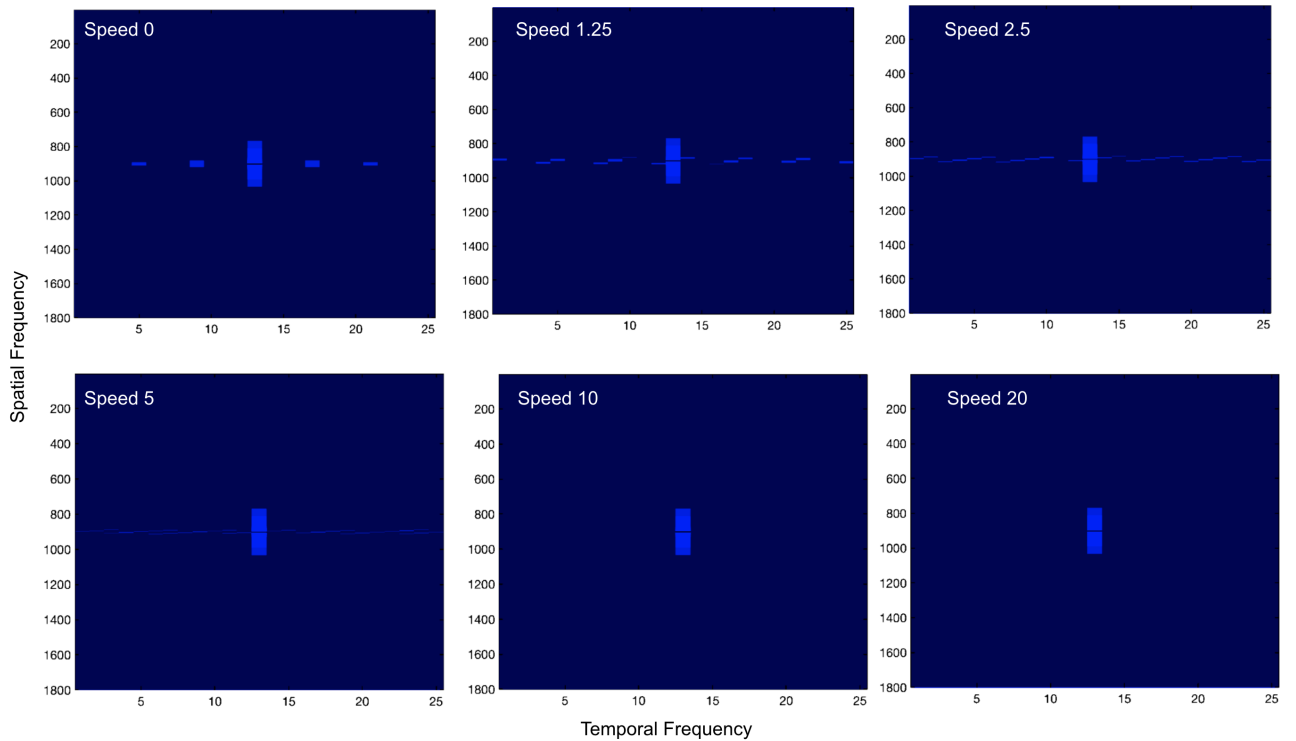


**Figure 8:** Fourier transform of the subsampled stimuli with 66ms ISI at 6 different speeds

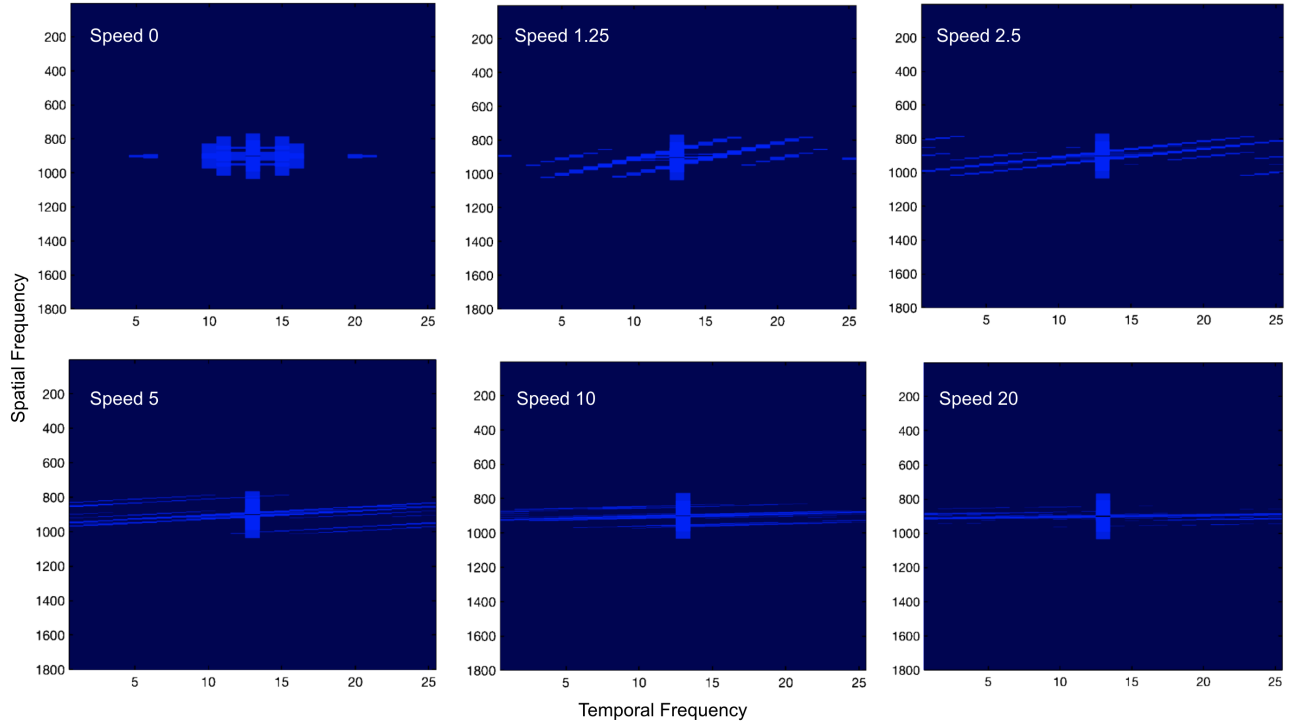


**Figure 9:** Fourier transform of the CPR stimuli with 66ms ISI at 6 different speeds

At this stage we already observe the temporal harmonics that are produced along the Fourier transform. These results already indicate that there are more information available to the visual system after being modulated in comparison to the stationary unmodulated condition at speed 0. The temporal harmonics are also seen along the temporal frequency axis. In the unmodulated stimuli condition, the temporal harmonics seem to increase as speed increases. In the subsampled condition, the temporal harmonics are also shown to be seen in evenly spaced intervals and diminish as speed increases. In the CPR condition, the temporal harmonics seems to be present at all speeds. These observations can be influential at the next stage of the study where the Fourier transform is combined with the WoV in order to find out exactly how much information is available to the human eye at each stage.

### 3.3 Combining the FT and WoV

At this stage, in order to have matching positive axis on both the FT and the WoV plots, we extracted the positive quadrant of each FT. Figure 10 is a zoomed in example of the extracted positive quadrant of the FT in the unmodulated condition. We then multiplied the positive quadrant of the matrix by the normalised WoV matrix in order to determine the available information about the stimulus that we can see.

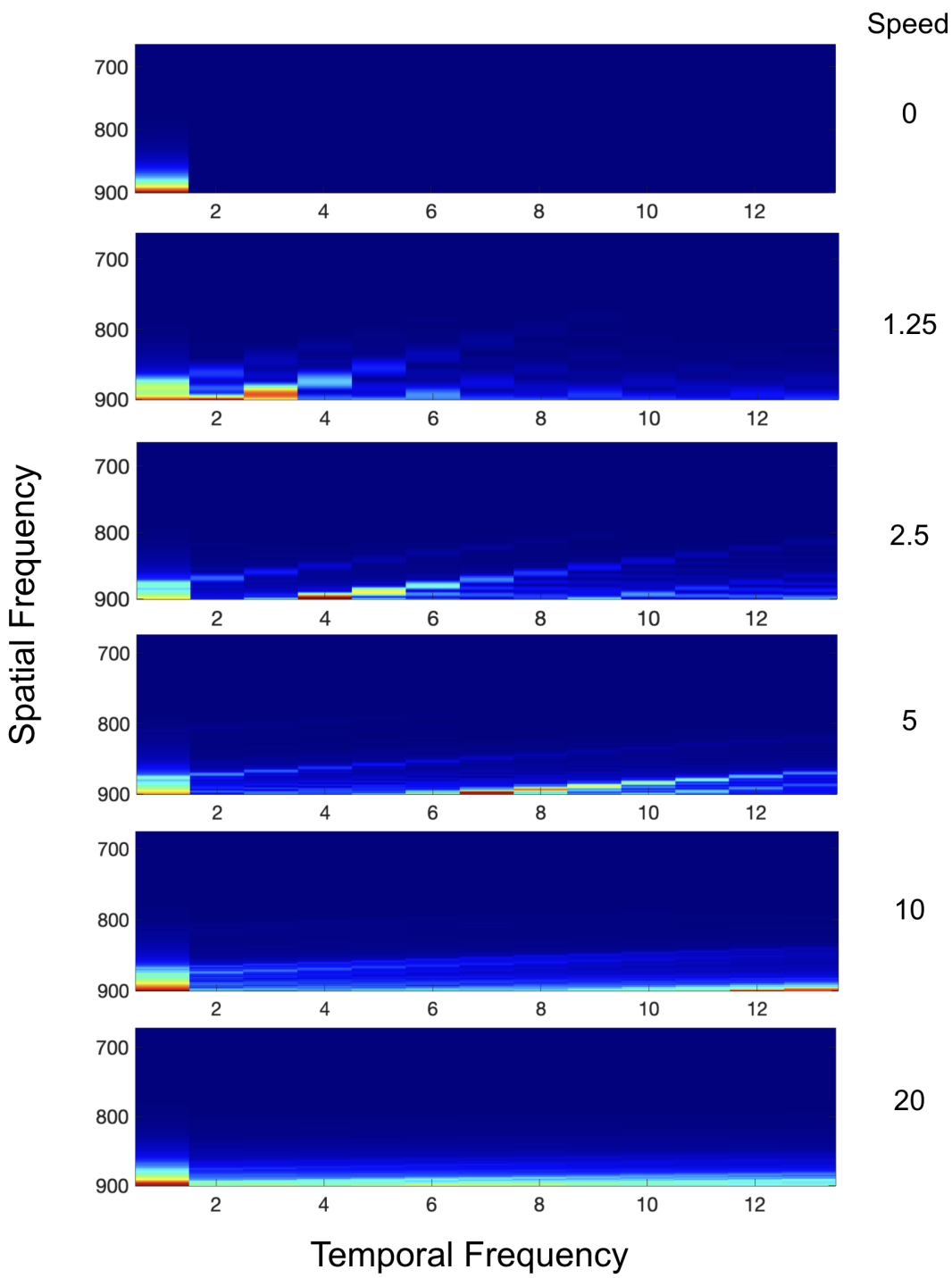


**Figure 10:** An example of the positive quadrant of the Fourier transform in unmodulated stimuli at the 6 different speeds

The results of the multiplication was a 2D matrix which was also collapsed into a single value by doing a sum of the entire 2D matrix for each trial and normalised with respect to the unmodulated speed 0 trial. These single values are an estimation of visibility for each condition and speed. Table 1 is the resulting estimate of visibility for each condition and speed.

**Table 1:** The table of estimate of visibility for all conditions

Condition	Modulation Condition	Speed					
		0	1.25	2.5	5	10	20
Unmodulated		1	0.389993845	0.381760764	0.39548496	0.427347308	0.338820896
Subsampled	0	1	0.389993845	0.381760764	0.39548496	0.427347308	0.338820896
	13	0.774433385	0.525165288	0.505970161	0.497097749	0.472338241	0.442033409
	26	0.831284224	0.589201369	0.579396885	0.569179884	0.531532005	0.530056044
	40	0.873653199	0.626338988	0.623802355	0.601729098	0.59240514	0.59033168
	66	0.934698819	0.681512699	0.642836741	0.650170664	0.683803254	0.645910218
CPR	13	0.570011446	0.498150151	0.432189732	0.416864181	0.339533828	0.346793632
	26	0.569693101	0.395656308	0.374519917	0.394936638	0.355496884	0.341254787
	40	0.569628475	0.386777186	0.352668493	0.363712104	0.380793863	0.34443895
	66	0.515595317	0.361317418	0.341065179	0.379786187	0.372900224	0.340919349
	106	0.507556436	0.348314671	0.334538808	0.359368096	0.428280465	0.340248272
	173	0.569307201	0.354537963	0.342210221	0.386518961	0.417749683	0.338687923

The results presented in Table 1 are used in order to compare the human data with the model performance, however, not all the data is compared. For the subsampled and the CPR conditions, the best score of the human performance was seen in the 66ms ISI modulation condition, therefore we chose to compare these data with our model estimations. Figure 11 is a plot of the model estimations (11A, 11C and 11E) against human data (11B, 11D and 11F). The x-axis shows the 6 different speed conditions whereas the y-axis is the score in human data and the estimation of visibility in the model performance. In this figure, in all three conditions, it is seen that the model estimations decrease at lower speeds with a slight increase around the 5-10ms speeds, however then continue to decrease at higher speeds, whereas the human data shows an increase in the unmodulated condition, an increase in the subsampled condition in higher speeds but a decrease in the lower speeds, and the CPR condition improves with in all the speeds.

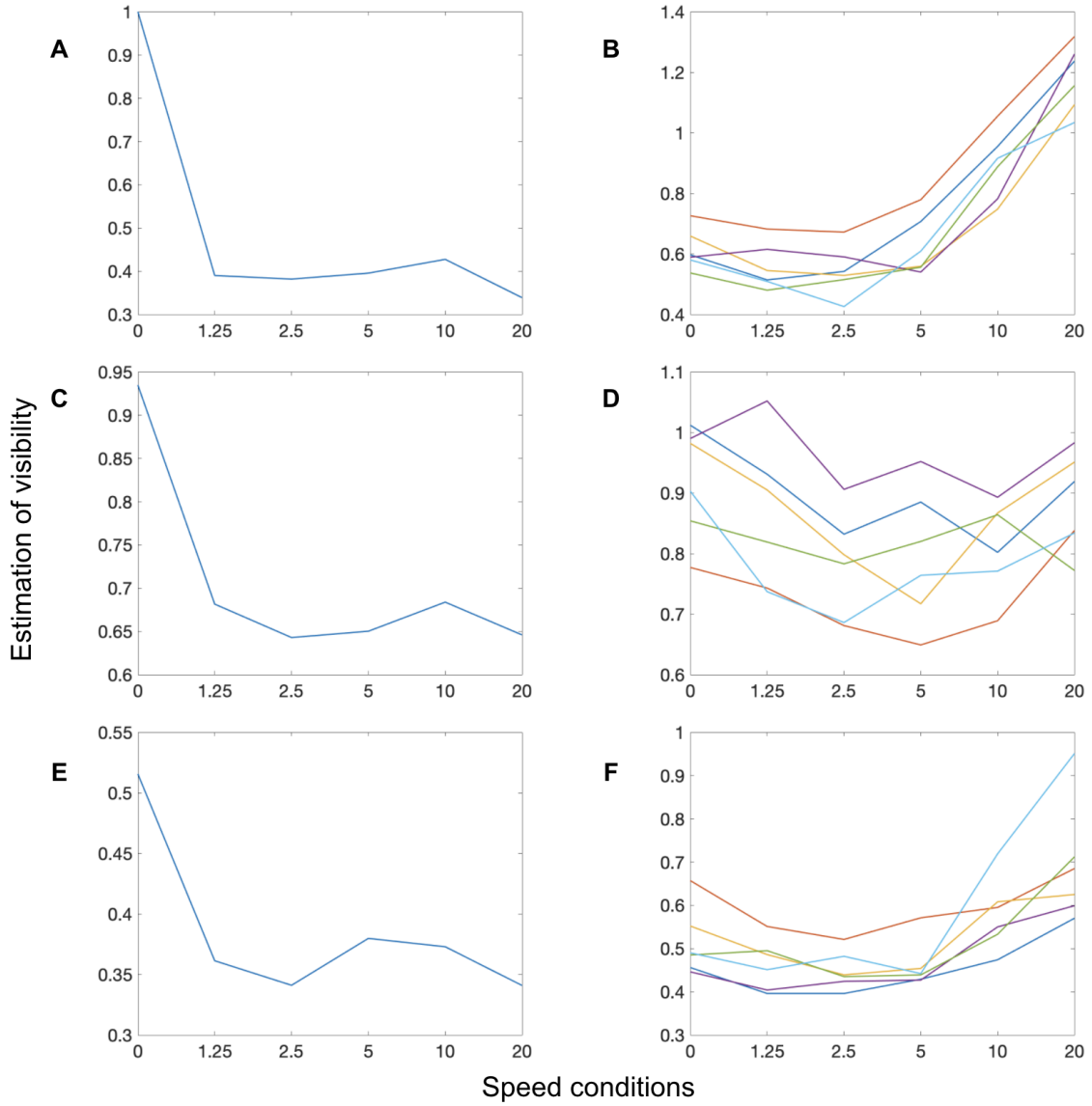


**Figure 11:** A comparison of the model estimation of visibility against human data; (A), (C) and (D) are the model estimations of visibility against (B), (D) and (F) which are plots of the human data. **Top:** Unmodulated stimuli **Middle:** Subsampled stimuli **Bottom:** CPR stimuli

## 4 Discussion

### 4.1 Summary

The aim of the study was to build a model of the visual system by modeling temporal modulations of different stimuli and combine it with the window of visibility to get an estimation of visibility for subsampled and CPR stimuli at different speeds. This was done to further confirm the findings of Patrick et al. (2019) that visual acuity is improved in patients with age-related macular disease when using contrast polarity reversed stimuli in all conditions. However when using subsampled stimuli, acuity was only improved in high speed conditions and vision was impaired in low speed conditions. We also attempted to further investigate whether the improvements in visual acuity were due to temporal harmonics created by the modulations of the target due to the wider range of spatio-temporal information of the stimuli. In the following section we will discuss the results of the model and aim to draw interpretations. We will discuss the inconsistencies found with our expectations and previous

findings and attempt to ascertain the reasons behind these inconsistencies. We will also assess the limitations of the model and suggest future directions for this field of research.

## 4.2 Interpretations, Limitations and Future Directions

The spatio-temporal threshold surface was successfully plotted and the Fourier transform of each trial was fit to the surface, and a single normalised value for estimation of visibility was generated as seen on Table 1. The results of the model suggest that in the unmodulated condition, the increase in the stimulus speed is associated with a decrease in visibility (Figure 11A), suggesting that vision is impaired in high speed stimuli. This decrease in the estimate of visibility is inconsistent with the human performances and the findings of Patrick et al. (2019) (Figure 11B). In the subsampled condition, for the low speed stimuli, the value of the estimate of visibility is decreased (Figure 11C), suggesting that vision is impaired in low speed subsampled stimuli. This goes in the same direction as the previous finding and the human data in (Figure 11D). However, with further increase of the speed, the performance in human data is improved, whereas the model tends to slightly improve but the improvement is not significant and at speed 20 the estimate of visibility is decreased again. Finally, in the CPR condition, the previous findings of human performances suggested that with an increase in the speed of the stimuli, vision will improve (Figure 11F). However, the model did not replicate these findings and we observed a decrease in the estimate of visibility as the stimuli speed increased (Figure 11E), indicating that with higher speed contrast reversed stimuli, visibility is lowered.

The main reason that comes to mind that might be causing the inconsistencies between the model performance and human data is that the model is created based on foveal vision, whereas the human data that has been collected is based on peripheral vision. Therefore, this model may not be the most suitable model to investigate peripheral acuity, however, it does provide the foundation for improving to a more complete model.

Previous findings in the field of vision had found that increasing the speed of the motion of visual stimuli is associated with lower visual acuity in general (Brown, 1972; Burr and Ross, 1982; Burr et al., 1986). Therefore we can interpret that the human performance might not only be caused by the higher speed of the stimuli, and that there might be other contributing factors, either external or internal, that can be influencing the performance of the subjects. The model estimated visibility to be lower in high speed stimuli in all three conditions which is an accurate finding in terms of what we expected. These findings suggest that the model has the potential to be an acceptable foundation of the visual system that can be improved with further experimentation and take into account for additional components of the visual system or external factors that affect vision with the aim of reaching a more complete model. For example contrast sensitivity heavily depends on object size (Chung and Legge, 2016). Therefore in future research, by manipulating the size of the stimulus and conducting the whole process repeatedly with different stimulus sizes in order to find the optimal perceivable stimulus size could be beneficial and result in a much more accurate representation of the human visual system. Other examples that can be similarly included in future models can include eccentricity, blur, brightness and exposure. Additionally, the model as a whole, performs well and consistent with the previous findings when at speed 0. This means that the model can perform well before motion is introduced, regardless of the temporal modulations of the stimuli, therefore by improving the model in order to have a more accurate response to motion we can see improvement regardless of the temporal modulations of the stimuli.

One of the important aspects of these results is that they confirm that temporal subsampling of the stimuli has different effects on peripheral acuity than contrast polarity reversal which goes hand in hand with the findings of Patrick et al. (2019). Subsampled stimuli seem to impair vision in lower speed stimuli, therefore using CPR as a method to go forward in this field is more plausible.

There can also be other factors that resulted in some inconsistencies with the human data. One reason could be that we only compared the modulation condition with 66ms ISI to human data in the subsampled and CPR conditions due to the fact that the subject performed best in these conditions. It could be possible that in other modulation conditions, the model estimations might be consistent with the human data, therefore we can make comparisons between the model and human data in every condition instead of just one.

In order to test the usefulness of the information available from the Fourier transform of the stimuli, we had to make sure that we used the information within the window of visibility, which meant that it could be seen by the human eye. However, the window of visibility in this experiment might not have been accurately modernised and did not result in the correct shape. This could then have led the results of the model to not represent the true estimation of visibility and therefore conflict with the human data.

According to Kelly (1979) lower spatial frequencies also face a shift in the contrast sensitivity function which might be constantly shifting the shape of the WoV when different spatial frequencies are presented to the eye. Therefore, by having a single plot of the spatio-temporal threshold surface for all the conditions and speeds, we might be limiting the fact that the contrast in those conditions may not match with the correct WoV for that condition.

In conclusion, the question that whether temporal harmonics improve peripheral acuity due to the fact that they increase the amount of information within the WoV and expose the retina to more information can be answered by future experimentation where the model has been improved and takes into account for further contributing factors, we can use the results of this study to build a more complete computational model of the visual system that includes more variables and artifacts.

## References

- Boi, M., Poletti, M., Victor, J. D., and Rucci, M. (2017). Consequences of the oculomotor cycle for the dynamics of perception. *Current Biology*, 27(9):1268–1277.
- Brown, B. (1972). Dynamic visual acuity, eye movements and peripheral acuity for moving targets. *Vision research*, 12(2):305–321.
- Burr, D., Ross, J., and Morrone, M. C. (1986). Seeing objects in motion. *Proceedings of the Royal society of London. Series B. Biological sciences*, 227(1247):249–265.
- Burr, D. C. and Ross, J. (1982). Contrast sensitivity at high velocities. *Vision research*, 22(4):479–484.
- Chung, S. T. and Legge, G. E. (2016). Comparing the shape of contrast sensitivity functions for normal and low vision. *Investigative ophthalmology & visual science*, 57(1):198–207.
- Crossland, M. D., Culham, L. E., Kabanarou, S. A., and Rubin, G. S. (2005). Preferred retinal locus development in patients with macular disease. *Ophthalmology*, 112(9):1579–1585.
- Demirel, S., Anderson, R. S., Dakin, S. C., and Thibos, L. N. (2012). Detection and resolution of vanishing optotype letters in central and peripheral vision. *Vision research*, 59:9–16.
- Falkenberg, H. K., Rubin, G. S., and Bex, P. J. (2007). Acuity, crowding, reading and fixation stability. *Vision Research*, 47(1):126–135.
- Kelly, D. H. (1979). Motion and vision. ii. stabilized spatio-temporal threshold surface. *Josa*, 69(10):1340–1349.
- Kumar, G. and Chung, S. T. (2014). Characteristics of fixational eye movements in people with macular disease. *Investigative ophthalmology & visual science*, 55(8):5125–5133.
- Martinez-Conde, S., Macknik, S. L., Troncoso, X. G., and Dyar, T. A. (2006). Microsaccades counteract visual fading during fixation. *Neuron*, 49(2):297–305.
- Nachmias, J. (1961). Determiners of the drift of the eye during monocular fixation. *Josa*, 51(7):761–766.
- Owen, C. G., Jarrar, Z., Wormald, R., Cook, D. G., Fletcher, A. E., and Rudnicka, A. R. (2012). The estimated prevalence and incidence of late stage age related macular degeneration in the uk. *British Journal of Ophthalmology*, 96(5):752–756.
- Patrick, J. A., Roach, N. W., and McGraw, P. V. (2019). Temporal modulation improves dynamic peripheral acuity. *Journal of vision*, 19(13):12–12.
- Peirce, J. W. (2007). Psychopy—psychophysics software in python. *Journal of neuroscience methods*, 162(1-2):8–13.
- Strasburger, H., Rentschler, I., and Jüttner, M. (2011). Peripheral vision and pattern recognition: A review. *Journal of vision*, 11(5):13–13.
- Watson, A. B. (2013). High frame rates and human vision: A view through the window of visibility. *SMPTE Motion Imaging Journal*, 122(2):18–32.
- Watson, A. B., Ahumada, A. J., and Farrell, J. E. (1986). Window of visibility: a psychophysical theory of fidelity in time-sampled visual motion displays. *JOSA A*, 3(3):300–307.

## 5 Appendix

### 5.1 MATLAB code

#### 5.1.1 WoV

```
function wov

w = 1:13;
a = 1:900;

[w, a] = meshgrid(w, a);

v = w./a;

a_max = 4./(v-0.1);
k = 25.89 + 28.46*abs(log((w./a)/3)).^3.034;
gout = k.*((w./a).*a.*exp(-2.*a./a_max));

% norm_gout = gout./max(gout);
%
% normalised = norm_gout.*positive;
%
% est = sum(normalised, 'all');
%
% figure;
% plot(normalised)
%
%
% figure;
% imagesc(normalised)

figure;
surf(w, a, gout)
set(gca,'Xscale','log')
set(gca,'Yscale','log')
set(gca,'Zscale','log')
xlabel('a');

end
```

#### 5.1.2 Fourier Transform of one unmodulated stimulus

```
for n=1:25
    image_{n} = imread(sprintf('%s.png',num2str(n)));
    G_{n} = rgb2gray(image_{n});
end

multi = cat(3,G_{1},G_{2:25});

F = fftn(multi);
S = abs(fftshift(F));
out = squeeze(mean(S,2));

figure;
imagesc(out)
```

## 5.2 Tables of all the original results

### 5.2.1 Unmodulated Results

Unmodulated Stimuli			
Speed	Real values	Normalised	Reveresed
0	20467.1877	1	1
1.25	52480.79673	2.564143033	0.389993845
2.5	53612.60145	2.61944153	0.381760764
5	51752.1266	2.528541164	0.39548496
10	47893.56875	2.340017078	0.427347308
20	60407.09978	2.951411825	0.338820896

### 5.2.2 Subsampled Results

Speed	Modulation Condition				
	0	13	26	40	66
<b>Real values</b>					
0	20467.1877	26428.59681	24621.16698	23427.13071	21897.09379
1.25	52480.79673	38972.84942	34737.16925	32677.49268	30031.99753
2.5	53612.60145	40451.37295	35324.98744	32810.37262	31838.85797
5	51752.1266	41173.36625	35959.08478	34013.95702	31479.71575
10	47893.56875	43331.63385	38506.03068	34549.30808	29931.39853
20	60407.09978	46302.35475	38613.25219	34670.65785	31687.35703
<b>Normalised</b>					
0	1	1.291266646	1.20295799	1.144618941	1.06986334
1.25	2.564143033	1.904162409	1.69721262	1.596579519	1.467324088
2.5	2.61944153	1.976401133	1.725932647	1.603071858	1.555604924
5	2.528541164	2.011676781	1.756913813	1.661877417	1.538057706
10	2.340017078	2.117126911	1.881354256	1.688033969	1.462408953
20	2.951411825	2.262272445	1.886592959	1.69396296	1.548202787
<b>Reversed</b>					
0	1	0.774433385	0.831284224	0.873653199	0.934698819
1.25	0.389993845	0.525165288	0.589201369	0.626338988	0.681512699
2.5	0.381760764	0.505970161	0.579396885	0.623802355	0.642836741
5	0.39548496	0.497097749	0.569179884	0.601729098	0.650170664
10	0.427347308	0.472338241	0.531532005	0.59240514	0.683803254
20	0.338820896	0.442033409	0.530056044	0.59033168	0.645910218

### 5.2.3 CPR Results

Speed	Modulation Condition					
	13	26	40	66	106	173
<b>Real values</b>						
0	35906.62582	35926.69046	35930.76644	39696.22499	40324.94962	35951.04304
1.25	41086.38263	51729.71414	52917.2568	56646.00335	58760.6248	57729.18512
2.5	47356.95041	54649.13013	58035.20329	60009.60795	61180.30911	59808.81461
5	49097.97629	51823.97817	56273.04528	53891.34307	56953.26864	52952.60967
10	60280.2608	57573.46581	53748.73309	54886.49874	47789.21616	48993.9036
20	59018.34927	59976.26541	59421.81544	60035.27739	60153.68586	60430.81635
<b>Normalised</b>						
0	1.754350737	1.755331069	1.755530216	1.939505592	1.970224255	1.756520904
1.25	2.007426875	2.527446121	2.585467901	2.767649576	2.870967212	2.82057242
2.5	2.313798608	2.670084964	2.835524067	2.931990894	2.98918982	2.922180394
5	2.398862854	2.532051738	2.749427333	2.63306048	2.782662156	2.587195196
10	2.945214638	2.812964178	2.626092744	2.681682484	2.334918547	2.393777998
20	2.883559293	2.930361821	2.903272121	2.933245069	2.939030352	2.952570585
<b>Reversed</b>						
0	0.570011446	0.569693101	0.569628475	0.515595317	0.507556436	0.569307201
1.25	0.498150151	0.395656308	0.386777186	0.361317418	0.348314671	0.354537963
2.5	0.432189732	0.374519917	0.352668493	0.341065179	0.334538808	0.342210221
5	0.416864181	0.394936638	0.363712104	0.379786187	0.359368096	0.386518961
10	0.339533828	0.355496884	0.380793863	0.372900224	0.428280465	0.417749683
20	0.346793632	0.341254787	0.34443895	0.340919349	0.340248272	0.338687923